

Recent Advancements in Si-Based Photonic Materials and Devices*

Yu Jinzhong[†] and Wang Qiming

(*Institute of Semiconductors, Chinese Academy of Sciences, Beijing 100083, China*)

Abstract: Silicon-based photonic devices, including stimulated emission from Si diodes, resonant cavity enhanced (RCE) photodiodes with quantum structures, metal oxide semiconductor (MOS) optical modulators with high frequency, SOI optical matrix switches and wavelength tunable filters, are reviewed. Emphasis is placed on our recent results for SOI-based thermo-optic waveguide matrix switches with low insertion loss and fast response. A folding re-arrangeable non-blocking 4×4 matrix switch with total internal reflection (TIR) mirrors and a first blocking 16×16 matrix were fabricated on SOI wafer. The extinction ratio and the crosstalk are excellent. The insertion loss and the polarization-dependent loss (PDL) at $1.55 \mu\text{m}$ increase slightly with longer device length, more bending, and more intersecting waveguides. The insertion losses are expected to decrease by $2 \sim 3 \text{dB}$ when anti-reflection films are added to the ends of the devices. The rise and fall times of the devices are 2.1 and 2.3 μs , respectively.

Key words: SOI; optical switch matrix; photodiodes; optical interconnection

EEACC: 2500

CLC number: TN25

Document code: A

Article ID: 0253-4177(2007)S0-0001-11

1 Introduction

The field of Si-based photonics has expanded and developed considerably since light emission from porous Si was reported in 1990^[1] and Si integrated optoelectronic circuits were proposed in 1993^[2]. The development of Si photonic components has found many applications such as optical communication, optical memory, optical interconnections in computers, and optoelectronic instruments.

Silicon is an indirect band gap material, which is not desirable for fabricating an efficient light-emitting device. Si has very weak electronic-optic effects, such as the Pockels effect, which inherently restricts Si as an optical material for fast modulation or waveguide devices. Silicon is transparent in the $1.3 \sim 1.6 \mu\text{m}$ wavelength range, and so it cannot be used as a detector material in this range. These disadvantages have limited the application of Si in photonics.

However, SOI has attracted increasing atten-

tion in recent years due to its excellent optical and electronic performance. SOI wafers with large size and high quality are commercially available. SOI-based photonics are perfectly compatible with standard microelectronics processes. High index contrast (~ 2) on SOI allows for small photonic devices and high photonic circuit density. Therefore, SOI electronic and photonic integration is possible.

Great advancements in SOI-based photonic devices have been made since the spring of 2004. A gigahertz (GHz) Si-based optical modulator^[3] and pulsed stimulated emission from a Si diode were successfully demonstrated^[4]. By using epitaxy and binding techniques, SiGe/Si RCE photodiodes (PD) with different structures such as multi-quantum wells (MQWs) and multi-quantum dots (MQDs) have been studied^[5]. A $1.55 \mu\text{m}$ Ge island RCE detector with a responsivity of 0.028 mA/W has been presented.

This paper focuses on our current results for SOI-based thermo-optic waveguide matrix switches. A folding re-arrangeable non-blocking 4×4

* Project supported by the National Natural Science Foundation of China (No. 60336010), the State Key Development Program for Basic Research of China (No. G2000-03-66), and the National High Technology Research and Development Program of China (No. 2002AA312060)

[†] Corresponding author. Email: jzyu@red.semi.ac.cn

Received 20 December 2006, revised manuscript received 5 January 2007

©2007 Chinese Institute of Electronics

matrix switch with TIR mirrors and blocking 8×8 and 16×16 matrixes were all fabricated. Both the extinction ratio and the crosstalk are excellent. The insertion loss and the polarization-dependent loss (PDL) at $1.55 \mu\text{m}$ increase slightly. The insertion loss decreases by $2 \sim 3 \text{ dB}$ when anti-reflection films are added to the ends of the devices. The rise and fall times of the devices are both about $2 \mu\text{s}$.

2 Progress of SOI photonic components and devices

2.1 Stimulated emission from a nanostructured Si pn junction diode^[4]

Light emitting from porous silicon, silicon nanocrystals, Si/SiO₂ superlattices, and erbium-doped silicon was reported. By introducing dislocation loops, an LED with η_{ext} of 10^{-3} was obtained. However, none of these approaches have been able to use current injection to achieve optical gain and stimulated emission. This difficulty was overcome recently by the use of nanostructured Si.

Non-uniform diffusion using spin-on dopant (SOD) with $4 \sim 20 \text{ nm}$ SiO₂ nanoparticles was employed to form pn junctions. SiO₂ was mixed with boron SOD to provide a non-uniform dopant source. The mixture was deposited on Si wafer, and then an array of boron p⁺-doped layers was formed by thermal diffusion. The ridge waveguide of $30 \mu\text{m}$ and the isolation layer outside the ridge provide confinement laterally for the optical field and the injection current, respectively, facilitating a gain-guided effect on the optical fields.

Stimulated emission was observed, with a pulsed (500ms, 50% duty cycle) threshold current I_{th} of 315mA and an external quantum efficiency (η_{ext}) of 0.013%. The entire spontaneous spectrum at 600 mA is suppressed, and two very large and very sharp peaks with 3nm half-width appear at 1214 and 1217nm. These results demonstrate optical gain and stimulated emission at bandgap energy (1.1eV) in a Si nanostructured pn junction diode at room temperature.

2.2 SOI based photodetector

SiGe/Si MQWs and Ge islands can be used as absorption layers in photodetectors, which can ef-

fectively improve the quantum efficiency and detect $1.3 \mu\text{m}$ and $1.55 \mu\text{m}$. The thickness of an absorption layer with SiGe/Si MQWs or Ge islands is so thin that an RCE structure is adapted to enhance the absorption. Light passes the absorption layer many times to increase absorbed power, as shown in Fig. 1.

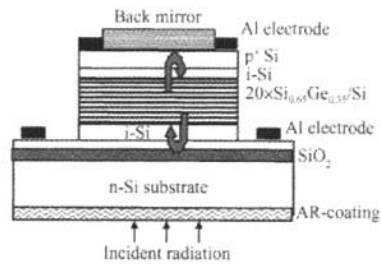


Fig. 1 Structure of SiGe/Si MQW RCE PD

SOI and a SiO₂/Si DBR (distributed Bragg reflector) can serve as reflectors^[5]. Bonding between SiGe epitaxial wafer and SiO₂/Si DBR on Si substrate is a good method to combine the epitaxial wafer with the bottom reflector mirror. The bottom-incident RCE-PD showed a responsivity of 44mA/W at $1.314 \mu\text{m}$, full width at half maximum (FWHM) of 6nm at a bias of 10V and η_{ext} of 4.2%.

Ge islands in a multilayer structure, which easily have an opto-response of $1.55 \mu\text{m}$ compared with the SiGe MQWs, are successfully grown on SOI substrates by optimization of the growth conditions. By introducing Ge quantum dots and a MOS tunneling structure to the device^[6,7], a $1.55 \mu\text{m}$ Ge island RCE detector with a responsivity of 0.028mA/W has been demonstrated. Compared with conventional PIN detectors, it has nearly threefold enhancement.

2.3 Optical wave guiding devices

Power splitters and combiners, optical switches and modulators, optical filters and attenuators, wavelength division multiplexers and demultiplexers are all waveguide devices. They play important roles in applications from optical fiber telecommunication to chip-to-chip optical interconnection. Among them, optical switches and modulators are core components for dense wavelength division multiplexing (DWDM), optical cross connection (OXC) and optical add/drop

multiplexing (OADM).

2.3.1 Optical modulator

Due to the absence of the linear electro-optic effect, optical modulation in Si is generally achieved through thermal effects or the free-carrier (FC) plasma dispersion effect. Though thermo-optical modulators with fast response were reported, the response speed of these devices is slow and limited approximately to the order of μs . To meet the demand of high-speed optical information processes, it is desirable to develop electro-optical modulators in SOI. The FC element generally consists of a p-i-n diode located laterally around a silicon waveguide. This phase-shifter obtained a modulation rate of $\sim 20\text{MHz}$ and $<0.1\text{dB}$ static excess loss. The FC phase-shifter causes full modulation for $\sim 10\text{mW}$ of electrical power dissipation.

By combining a DBR with a p-i-n structure, a DBR optical modulator was fabricated and a fast modulation with a speed as high as 1.4GHz was achieved^[8]. The DBR structure also finds applications in Fabry-Perot cavity optical modulators. The modulation region is made of an F-P micro-cavity, with DBRs arranged along both access ends. The reported device has a total length as short as $20\mu\text{m}$ and a direct current (DC) power consumption as low as $25\mu\text{W}$, with a good tradeoff between modulation depth (80%) and transmittivity (86%)^[9,10].

Another modulation structure, the bipolar mode field effect transistor (BMFET) optical modulator^[11], is based on optical field absorption. A drain was added to the traditional p-i-n structure, thus forming a BMFET. The modulation is achieved by adjusting the distribution of carriers, instead of their generation and recombination. Thus a high modulation speed is easily realized.

A novel charge-inducing optical modulator based on MOSFET was recently reported^[3]. It was made on SOI substrate with a rib waveguide structure (Fig. 2). It is still a Mach-Zehnder interferometer (MZI), and the free-carrier plasma effect is adopted to realize the phase modulation. In a MOS structure, a driving voltage evokes an accumulation of charges near the gate dielectric of the capacitor, which change the refractive index profile of the modulation area and consequently the optical phase of light passing through the

waveguide. Therefore, the device is voltage-modulated instead of current-modulated, and the main transportation process of carriers is an electric field-driven drift process, instead of the diffusion process. The modulation speed is increased dramatically up to 1GHz , without limitation of carrier combination in silicon.

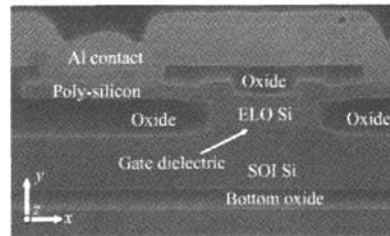


Fig. 2 SEM cross-section of the phase shifter^[12]

Through improvements in material quality, device design, and driver circuits, a MOS-capacitor-based modulator on SOI wafer with unprecedented performance was demonstrated by Dr. Liao and his colleagues of Intel Corporation^[12]. An estimated intrinsic bandwidth (as measured by RC cutoff) of 10GHz and driver-limited near rail-to-rail data transmission at 10Gbps with 3.8dB extinction ratio (ER) were reported in April 2005. As shown in Fig. 2, there is $1\mu\text{m}$ of n-type doped crystalline Si on the bottom of the rib waveguide, which is the top silicon layer of the SOI wafer. Different from the first version of the device employing poly-crystal silicon (poly-Si), $0.55\mu\text{m}$ of p-type doped crystalline Si is deposited on the top of a 10.5nm gate dielectric, a multi-layer stack of silicon dioxide and nitride, which is significantly less lossy than poly-Si for good material performance. Here, a process called epitaxial lateral overgrowth (ELO) is used. All waveguide dimensions here are smaller than the first version of the device, and consequently the optical mode is more tightly confined and interacts more strongly with the charges. Therefore, the modulation efficiency of the phase-shifter is improved with more than 50% reduction in the product $V_\pi L_\pi$, which meets the requirement to achieve a π -radian phase shift.

2.3.2 Optical switch

A silicon waveguide integrated optical switch with microsecond switching speed was reported in

OFC 2003^[13]. Till now, most optical switches employ the thermo-optical effect. The high thermal conductivity of silicon means that the switching time was $\sim 10\mu\text{s}$ for the thermo-optic device. This switching time can be reduced to less than $1\mu\text{s}$ for a free carrier-based device at the expense of $\sim 0.25\text{dB}$ extra excess loss.

Both thermo-optical and electro-optic switches were successfully made in our laboratory^[14]. For 2×2 thermo-optical switch, an extinction ratio of 12dB, insertion loss of 18dB, consumption power of 190mW, and switch time of 10ms were achieved. A rearrangeable nonblocking thermo-optic 4×4 switching matrix operating at $1.55\mu\text{m}$ was designed and fabricated using an SOI waveguide system. The matrix is composed of five 2×2 multimode interferometer (MMI)-MZI switch elements, which result in a smaller device size than the conventional crossbar and tree architecture. The measured crosstalk is between -12 and -19.8dB . The power consumption of each switch element is about 150mW. The switching time of a switch element in the matrix is less than $10\mu\text{s}$.

2.3.3 1.3 μm Si-based tunable optical filter

By adding a Fabry-Perot cavity to MEMS, a $1.3\mu\text{m}$ Si-based tunable optical filter has been fabricated by precisely controlling the length of the cavity and thicknesses of Si/SiO₂ multiple films. The cavity length and the refractive index can be changed by an applied voltage so that the wavelength is tunable. Its performance was found to be as follows: Its operating wavelength is around $1.3\mu\text{m}$, tunable range is $> 23\text{nm}$, power consumption is $\sim 23\text{mW/nm}$, line width is 0.5nm (near $1.3\mu\text{m}$) and peak-valley ratio is 22dB.

3 Our recent results and innovations

Based on accurate simulation tools, we designed and fabricated single mode rib waveguides, multimode interference couplers, and optical matrix switches on SOI by both anisotropic wet etching and inductively coupled plasma (ICP) reactive ion etching (RIE).

3.1 Propagation simulation of SOI rib waveguides and single mode conditions

Single mode operation is strictly required for

most optical waveguide devices. In order to design devices accurately, we determined the single mode conditions of silicon rib waveguides with different cross-sections utilizing home coded simulation tools.

Two kinds of wide-angle BPM with high computation efficiency are proposed. One utilizes the least-squares expansion approximation^[15]. According to the rib waveguide, the eigenmode near cutoff will expand horizontally (in the x -direction) deeply into the side slabs. Thus an ultra-wide computation window is necessary. In order to reduce the computation resource demand and increase the efficiency, a non-uniform discretization of the physical area is used in our simulation. The other introduces a preconditioner in the iterative procedure to make the computation efficiency ten times higher^[16]. When the first order mode of the rib waveguide is solved by use of imaginary distance BPM, an ultra long propagation distance is necessary. To reduce the computation time of the ultra-long propagation, we increase the propagation step during computation. The validity of the increasing steps is ensured by the stabilizing of the mode profile along with the increasing of the propagation distance. The results of numerical simulation show that the mode matching technique is more accurate than the effective index method (EIM) for getting single-mode conditions.

We can obtain the whole single mode condition by changing the structural parameters of the rib waveguide and repeating the above mentioned procedure, the results of which are shown in Fig. 3. Through numerical fitting of the stricter curve of the TM mode, we get the same equation as reported by Soref *et al.*^[17]. The single-mode condition for an SOI rib waveguide with a rectangular cross-section is given by^[18]

$$t \leq 0.29 + \frac{r}{\sqrt{1 - 0.97r^2}}, \quad r > 0.5 \quad (1)$$

where $t = w/H$, $r = h/H$, w , H and h are the width, height, and slab height of the rib waveguide, respectively.

In order to describe the slope index interface accurately, a new seven-point discretization scheme is proposed^[16]. Using the same numerical method described above, we obtained the single-mode condition for an SOI rib waveguide with a

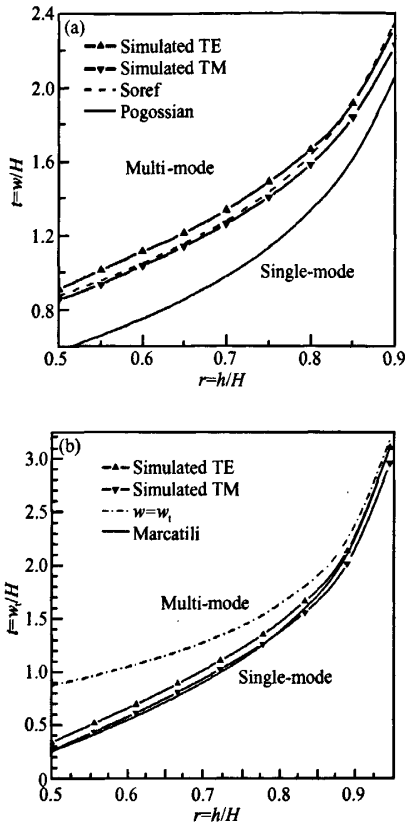


Fig. 3 Simulated single mode condition of the rib waveguide with rectangular cross-section (a) and trapezoidal cross-section (b)

trapezoidal cross-section, as shown in Fig. 3 (b)^[19]. By numerical fitting of the stricter curve of the TM mode, an equation is obtained as

$$t \leq -1.12 + \frac{0.63r}{\sqrt{1-1.03r^2}} + 2.04r, \quad r > 0.5 \quad (2)$$

where $t = w_t/H$, w_t is the top width of the rib waveguide and the slope angle of the trapezoid is 54.74° . Both of the above single mode conditions have been used in our device designs.

3.2 Spot size converter (SSC) and SOI optical matrix switches with SSC

Coupling light into and out of a silicon chip is very challenging due to the large mode mismatch between SOI single mode waveguides and standard fibers. One way to overcome the large differences in effective index, core size and symmetry is to use a tapered waveguide. The results using a pseudo-

vertical taper structure, formed by selective single-crystal epitaxial silicon overgrowth, have given coupling losses as low as 0.5dB/facet^[20]. Figure 4 shows a schematic diagram of the spot size converter in the input and output ports used to expand the optical mode from the SOI single mode waveguide to match the optical fiber mode. In our device, the spot size converter structure is formed by ICP-RIE twice, and it has a uniform height but varying width. The length of the taper is 1.5mm, long enough to make the transmission loss of the SSC negligible (less than 0.03dB). When the optical field propagates along the SSC, the energy is “squeezed” to the lower part of the SSCs gradually and is only distributed in the nether rib and the slab waveguide at the end of the SSC. For perfect alignment, the calculated coupling loss of the SSC is approximately 0.44dB. Measurement shows the loss of the SSC is 1.81dB, including transmission loss, coupling loss and reflection loss.

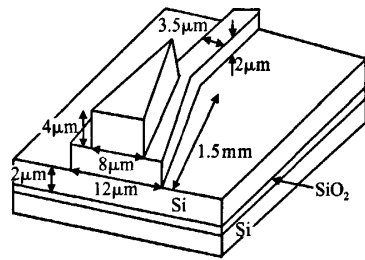


Fig. 4 Schematic diagram of spot size converter

SOI thermo-optical matrix switches, integrated with SSCs in input and output ports, are fabricated. For a 2×2 switch, the insertion loss and polarization-dependent loss (PDL) for wavelengths in the range of 1540~1560nm are 8 ± 1 dB and less than 1.5dB, respectively. At 1550nm, the PDL is less than 0.5dB; the crosstalk is -17.71 dB or -18.45 dB, and the extinction ratio is 18.28dB or 19.11dB when light is imported from different ports. As for the 4×4 blocking switch array, it shows a performance of insertion loss of 12.5~13.5dB, crosstalk of $-17.5 \sim -14$ dB, and extinction ratio of 16~22dB. As to the 4×4 rearranged non-blocking switch array, the insertion loss and PDL are less than 10dB and 1dB, respectively. The extinction ratio is larger than 18dB. For the 8×8 blocking switch array, the insertion loss and PDL are less than 14dB and 2dB, respectively. The

crosstalk is less than -18dB , and the extinction ratio is close to 20dB or larger^[21].

3.3 Isolating grooves

The structure of the switch element is shown in Fig. 5. The function of the isolating grooves parallel to the waveguide in the SOI device is to prevent lateral heat diffusion, decrease power consumption and crosstalk, prevent coupling of different waveguides, etc. Mode coupling between the two arms which are close to each other breaks the independence of split light and degrades the extinction ratio. To avoid such coupling, a deeply etched isolating groove is introduced to prevent cross coupling between the two neighboring MZI arms, as shown in Fig. 6. The coupling is very small because the groove is etched down to the buried oxide. Another important advantage of the trench is to isolate the heat transfer between the arms. This will reduce the switching power greatly, as was proved by our results of simulation and experiment.

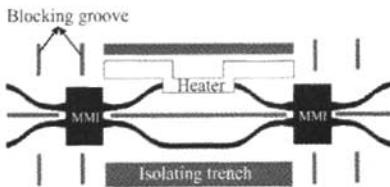


Fig. 5 Structure of switch element

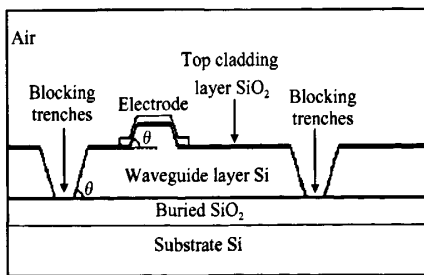


Fig. 6 Cross-section of the phase-shifting arm

Those grooves vertical to the waveguide are also deeply etched to prevent dispersion of the light of the chip. When the laser beam from a single mode fiber is input into the single mode silicon rib waveguide, not only the fundamental mode but also the radiation modes will be excited. These radiation modes will lead to stray light in the chip. Simultaneously, stray light will be induced by the

surface scattering. This useless stray light will degrade the performance of the device and make the measurement more difficult. The blocking groove will reflect the stray light and let it escape from the device chip.

Comparison between characteristics of an 8×8 blocking switch matrix with parallel grooves and one without grooves shows that the crosstalk can be decreased from $-17 \sim -14\text{dB}$ to less than -18dB . The power consumption and response time are both decreased^[22]. The response time at the rising and the falling edges are 4.6 and $1.9\mu\text{s}$. The power consumption of the switch cell with grooves is about 200mW ^[21].

3.4 16×16 SOI optical switch matrix

Among the three kinds of topological structures for matrix switches, the blocking matrix requires the least number of cells. A blocking 16×16 optical switch matrix that is 4.5cm long and 2.15mm wide is made by ICP-RIE, which is composed of 32 switch units through 4-stage interconnections, as shown in Fig. 7. The fabrication difficulty of these switches is reduced because the number of switch cells is much smaller than that of the non-blocking matrix. The length of each 2×2 switch unit is 0.6cm , and the width is only $120\mu\text{m}$. The isolating and blocking grooves are also used in the optical matrix switches. In order to enhance the coupling efficiency between the single mode fiber and input waveguide, the thickness of the top silicon layer is selected to be $8\mu\text{m}$ and the spot size converter in the input and output ports is designed as described in the preceding text. The last results of our experiments show that the insertion loss measured is $21.7 \sim 27.1\text{dB}$ and the crosstalk is $-12.6 \sim -33.2\text{dB}$. The extinction ratio is $13.8 \sim 22.3\text{dB}$, and the power consumption is about 200mW . The matrix also shows characteristics of fast response with rise time and fall time,

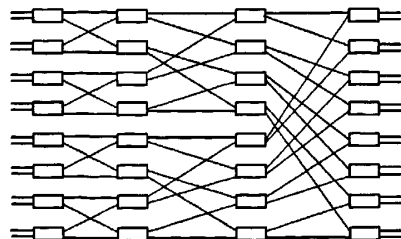


Fig. 7 Topological structure of 16×16 optical matrix switches

2. 1 and 2. 3 μ s respectively, as shown in Fig. 8 and Fig. 9. This is also the largest scale SOI blocking optical switch matrix that has been reported.

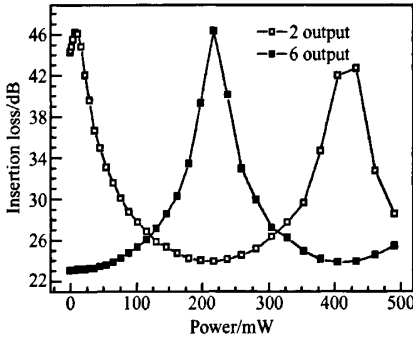


Fig. 8 Insertion loss of 16 \times 16 switches versus heating power

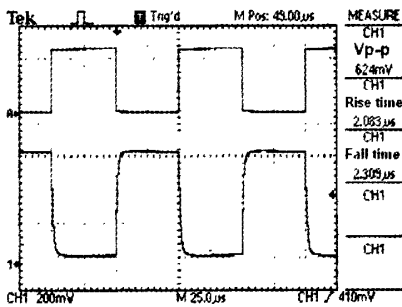


Fig. 9 Switching characteristics of 16 \times 16 switches

3.5 Performance of S-shaped bend waveguide and reflection mirrors

The crosstalk characteristics in S-shaped intersection waveguides are related to their cross-sections. For intersection waveguides with large cross-sections, the radiation loss of bend waveguide is larger-“crosstalk arises from loss”; the larger bend radius is, and the smaller intersecting angle is, the better the crosstalk performance is. On the other hand, if the waveguide cross-sections are reduced, the effective index difference will increase, light confinement will be stronger, and the optical radiation loss in the bent waveguide will also decrease. The widening in the intersect connection waveguide increases crosstalk-“loss arises from crosstalk”; the smaller bend radius is, and the larger the intersecting angle is, the better the crosstalk performance is.

To overcome the disadvantages of conven-

tional structure, we present and fabricate a novel folding matrix optical switch in which switch elements are connected by TIR mirrors instead of S-bends. Compared to the conventional matrix shown in Fig. 7, the novel matrix has a very compact structure, and all intersection angles are 90°, as shown in Fig. 11, which can eliminate bend loss and reduce crosstalk the most. The wafer used here is (100)-oriented SOI. The waveguides are along the $\langle 110 \rangle$ crystalline direction of the wafer, while underetched vertical walls in the $\langle 100 \rangle$ direction designed as mirrors are naturally perpendicular to the wafer surface. The scattering derived from rough mirror surfaces is the greatest factor in excess loss of mirrors. Thus the wet etching is usually employed to fabricate very smooth mirror surfaces. The SEM image of TIR mirror is shown in Fig. 10. The figure denotes that an excellent mirror with a smooth and vertical facet was obtained. In our experiment, the roughness of the mirror facet as determined by AFM is about 1.49nm^[29].

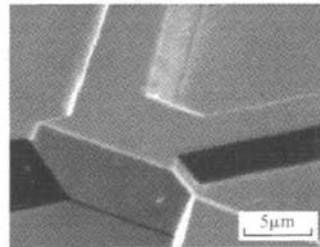


Fig. 10 SEM image of TIR mirror

3.6 All wet etching process and folding SOI optical switch matrix

In order to achieve smooth interfaces with less scattering loss of the propagating light beam, especially in small scale waveguides, anisotropic chemical wet etching of silicon can be employed in the fabrication process. The RMS roughness of interfaces by wet-etching is less than 2nm, much smaller than that of ~ 10 nm order by conventional dry-etching methods. Thus the scattering loss proportional to the cube of the interface roughness is reduced greatly. At the same time, the chemical etching is very inexpensive and easy to control with a high accuracy of etching depth that is as small as 50nm.

Different kinds of devices can also be fabri-

cated by wet etching, including smooth-side rib waveguides with a trapezoidal cross-section, vertical mirrors, MMIs, VOAs and 2×2 switches, etc. As results that we have obtained^[24], the extinction ratio of a 2×2 thermo-optical switch is 17.1 dB, and the power consumption is 235 mW. The response time is $8 \mu\text{s}$ while the insertion loss is 12 dB. After optimization, the extinction ratio can reach 20 dB, and the power consumption falls down to only 145 mW, while the rise and fall times are 7.5 and 6.7 ms, respectively.

An integrated folding 4×4 Benes rearranged switch^[22] and a 4×4 simplified tree nonblocking switch^[25] are made by wet etching with areas of $20 \text{ mm} \times 1.6 \text{ mm}$ and $20 \text{ mm} \times 3.2 \text{ mm}$, respectively. The folding structure of the Benes matrix is shown in Fig. 11. The range of insertion loss and crosstalk is 23.9 to 25.3 dB and -16.3 to -18.1 dB, respectively, depending on different transmission route. This is the first time that wet etching has been adopted to fabricate a switch matrix, and it is also the first time a folding switch matrix has been made on SOI material^[23]. It is also the largest nonblocking switch based on SOI that has been reported^[26].

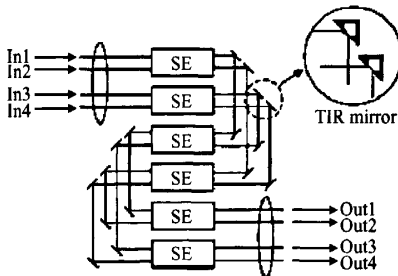


Fig. 11 Novel folding 4×4 Benes matrix switch

3.7 Self-aligned methods and combining wet and dry etching to fabricate an optical switch matrix

As shown in published papers, we demonstrate an average excess loss of -1.1 dB per mirror^[24]. However, the positions and orientations of mirror pairs in the optical circuits are different from each other, with the result that it is not easy to get perfect mirror facets together in our old designs without applying any alignment methods, which could cause additional excess loss of mirrors. Since the fabrication of TIR mirrors has strict requirement regarding photolithography er-

rors, we proposed a new self-aligned design to overcome this difficulty. In experiment, the waveguides are made by ICP dry etching while the mirrors are fabricated by anisotropic wet etching.

In this design, as shown in Fig. 12, the first mask defines waveguides and a hollow trigonal area (see Fig. 12 (a)). The open room of the trigonal area is designed for following etching. The second mask is used to open a window on the top of the hollow trigonal area. The size of the former is a little bigger than the latter so that the trigonal room in the first mask can be revealed in the window (see Fig. 12 (b)). In the process, the first mask must be maintained till the completion of mirror etching. The dashed line designates the final position of the mirror facet. The final positions of mirrors were dependent on the first mask in the design. Because all the sizes of the trigonal areas in the first mask are identical, the final relative positions should be in accord with one another even if the photolithography errors in the fabrication could not be neglected. Therefore, the excess loss from the position difference of the mirrors can be eliminated if the etching process of the mirrors is controlled accurately.

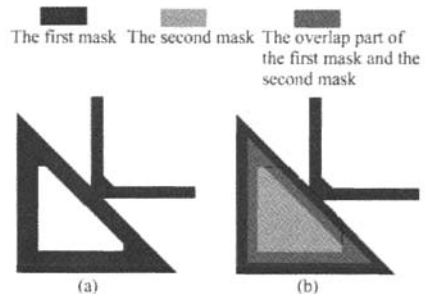


Fig. 12 Self-aligned design of the TIR mirror

By improvement in design, optimization of parameters, and the self-alignment method, the fabrication tolerance of mirrors increases from 1 to $3 \mu\text{m}$ and the excess loss of switch unit decreases from 2.4 to 1.0 dB. At the same time, the average loss of the switch matrix also decreases from 25 to 21 dB and the crosstalk falls to -22 from -18 dB. The performance of the device is improved while the process difficulty is reduced.

3.8 Strong confinement MMI coupler

A strong confinement MMI coupler is pro-

posed and designed. Deep etching is used in the multi-mode region while other regions retain shallow etching to meet the single mode condition. By a simple self-alignment method, waveguides with different rib heights are designed in one layout. In this way, photolithographic error can be lost. We successfully fabricated strong confinement general MMI couplers and paired ones. The largest excess loss is 4.9dB and the worst uniformity is 0.03dB^[26].

3.9 Ge island RCE detector with high-reflectivity bottom mirror

Due to their opto-response in the range of $1.3 \sim 1.55\mu\text{m}$, SiGe/Si MQWs and Ge MQDs (nano islands) have become potential candidates for future optical fiber communication. In our team, research work focuses on the design of RCE detectors and the epitaxy of high quality Ge nano islands and undulated SiGe/Si MQWs.

For the RCE detector, one of the key techniques is to fabricate high-reflectivity bottom mirrors. In our paper, we have reported a novel and simple method to prepare the mirrors in the back hole^[27,28] of the silicon slice using the etching-stopped technology of the buried SiO₂ in the SOI substrate. First, $1\mu\text{m}$ thick SiO₂ was deposited at low temperature by plasma-enhanced chemical vapor deposition (PECVD) on both sides of the slice as mask layers. With the buried SiO₂ as etching-stop layer, the back hole with the smooth bottom surface is formed by standard photolithography technology and etched in ethylenediamine-pyrocatechol-water (EPW) solution at another low temperature. In the back hole, 5 pairs of SiO₂/Si DBRs with amorphous Si (93nm) and SiO₂ (220nm) were deposited by e-beam evaporation as high quality bottom mirrors.

As shown in Fig. 13, in the range of $1.2 \sim 1.55\mu\text{m}$ a reflectivity of more than 99% of the bottom DBR in the hole was obtained. The small difference between the reflectivity of the mirror out of the hole and in the hole is likely to originate from the influence of the cavity formed by the buried SiO₂ and the mirror grown out of the hole.

The Ge islands in multilayer structure, which easily have the opto-response of $1.55\mu\text{m}$ compared with the SiGe multi-quantum wells, are suc-

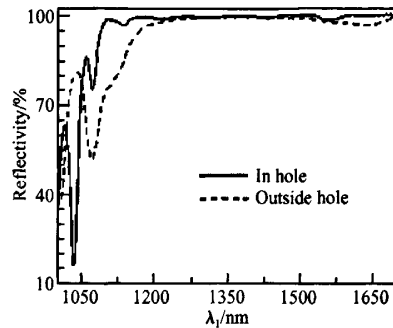


Fig. 13 Reflectivity spectrum of bottom DBR grown in and out of hole

cessfully grown on SOI substrates by optimization of the growth conditions. A $1.55\mu\text{m}$ Ge island RCE detector has been fabricated with enhanced quantum efficiency of the detector by bottom mirrors. The cut-in and the breakdown voltages of the device are about 0.35 and -65V , respectively. The dark current density at 5V reverse bias is measured to be $5.1 \times 10^{-7} \mu\text{A}/\text{mm}^2$. The peak responsivity of the detector at 1543.8nm is $0.028\text{mA}/\text{W}$, and the FWHM is 5nm. Compared with the responsivity of a $0.01\text{mA}/\text{W}$ of p-i-n Ge island detector without high reflectivity bottom and top mirrors, the responsivity of the RCE detector is enhanced nearly three times.

4 Conclusion

Research on SOI optical waveguide devices has been a focus in recent years. Using accurate simulation tools, we designed and fabricated single mode rib waveguides, MMI couplers, and optical matrix switches on SOI by both wet etching and dry etching. In addition, SiGe/Si MQWs and Ge island RCE detectors with high-reflectivity bottom mirrors for $1.55\mu\text{m}$ operation were fabricated successfully. In the future, we will optimize all of the present devices and design larger scale structures. By advanced process technology and higher quality SOI wafer, we expect to obtain improvements in the performance of these devices. Great advancements in SOI-based photonic devices made in the past two years were exciting and greatly promising. It is predicted that SOI-based photonics will be key elements in optical information processing.

References

- [1] Canham L T. Silicon quantum wire array fabrication by electrochemical and chemical dissolution of wafers. *Appl Phys Lett*, 1990, 57; 1046
- [2] Soref R A. Silicon-based optoelectronics. *Proc IEEE*, 1993, 81; 1687
- [3] Liu A, Jones R, Liao L, et al. A high-speed silicon optical modulator based on a metal-oxide-semiconductor capacitor. *Nature*, 2004, 427; 615
- [4] Chen M J, Yen Y L, Li J Y, et al. Stimulated emission in a nanostructured silicon pn junction diode using current injection. *Appl Phys Lett*, 2004, 84(12); 2163
- [5] Yu Jinzhong, Li Cheng, Cheng Buwen, et al. Getting and defect engineering in semiconductor technology. In: Richter H, Kittler M. GADEST Scitec Publication, 2003; 255
- [6] Hsu B C, Chang S T, Chen T C, et al. A high efficient 820nm MOS Ge quantum dot photodetector. *IEEE Electron Device Lett*, 2003, 24(5); 318
- [7] Liu C W, Liu W T, Lee M H, et al. Novel photodetector using MOS tunneling structures. *IEEE Electron Device Lett*, 2000, 21(6); 307
- [8] Sciuto A, Libertino S, Alessandria A, et al. Design, fabrication, and testing of an integrated Si-based light modulator. *J Lightwave Technol*, 2003, 21(1); 228
- [9] Irace A, Breglio G, Cutolo A. All-silicon optoelectronic modulator with 1GHz switching capability. *Electron Lett*, 2003, 39(2); 232
- [10] Barrios C A, Almeida V R, Panepucci R R, et al. Compact silicon tunable Fabry-Perot resonator with low power consumption. *IEEE Photonics Technol Lett*, 2004, 16(2); 506
- [11] Barrios A, Almeida V R, Lipson M. Low-power-consumption short-length and high-modulation-depth silicon electrooptic modulator. *J Lightwave Technol*, 2003, 21(4); 1089
- [12] Liao L, Samara-Rubio D, Morse M, et al. High speed silicon Mach-Zehnder modulator. *Opt Express*, 2005, 13(8); 3129
- [13] House A, Whiteman R, Kling L, et al. Silicon waveguide integrated optical switching with microsecond switching speed. *OFC Technical Digest*, 2003, 2; 449
- [14] Yu Jinzhong, Xia Jinsong, Fan Zhongcao, et al. Proceedings of Third Joint Symposium on Opto- and Microelectronic Devices and Circuits, Wuhan, 2004; 47
- [15] Soref R A, Schmidtchen J, Petermann K. Large single mode rib waveguides in GeSi-Si and Si-on-SiO₂. *IEEE J Quantum Electron*, 1991, 27(8); 1971
- [16] Day I, Evans I, Knights A, et al. Tapered silicon waveguides for low insertion loss highly-efficient high-speed electronic variable optical attenuators. *Opt Fiber Commun*, 2003, 1; 249
- [17] Xia J S, Yu J Z. A new beam propagation method based on least-squares expansion approximating. *Acta Physica Sinica*, 2003, 52(3); 515
- [18] Xia J S, Yu J Z, Li Y P, et al. Single-mode condition for silicon rib waveguides with large cross sections. *Opt Eng*, 2004, 43(9); 1953
- [19] Xia J S, Yu J Z. New finite-difference scheme for simulations of step-index waveguides with tilt interfaces. *IEEE Photonics Technol Lett*, 2003, 15(9); 1237
- [20] Xia J S, Yu J Z. Single-mode condition for silicon rib waveguides with trapezoidal cross-section. *Opt Commun*, 2004, 230(4~6); 253
- [21] Li Yanping, Yu Jinzhong, Chen Shaowu. Rearrangeable non-blocking SOI waveguide thermo-optic 4 × 4 switch matrix with low insertion loss and fast response. *IEEE Photonics Technol Lett*, 2005, 17(8); 1641
- [22] Liu J W, Yu J Z, Chen S W, et al. Integrated folding 4 × 4 optical matrix switch with total internal reflection mirrors on SOI by anisotropic chemical etching. *IEEE Photonics Technol Lett*, 2005, 17(6); 1187
- [23] Liu J W, Yu J Z, Chen S W. Novel folding large-scale optical switch matrix with total internal reflection mirrors on silicon-on-insulator by anisotropy chemical etching. *Chinese Physics Letters*, 2005, 22(1); 142
- [24] Liu J W, Yu J Z, Chen S W, et al. Fabrication and analysis of 2 × 2 thermo-optic SOI waveguide switch with low power consumption and fast response by anisotropy chemical etching. *Opt Commun*, 2005, 245(1~6); 137
- [25] Liu Jingwei, Yu Jinzhong, Chen Shaowu, et al. Design and fabrication of compact nonblocking 4 × 4 optical matrix switch on SOI by anisotropy chemical etching. *Opt Eng*, 2005, 44(7); 070503
- [26] Yang D, Li Y P, Sun F, et al. Fabrication of a 4 × 4 strictly nonblocking SOI switch matrix. *Opt Commun*, 2005, 250(1~3); 48
- [27] Li C B, Li H X, Mao R W, et al. Fabrication of low-cost and high-reflectivity bottom mirrors for Si-based micro-cavity devices. *Electron Lett*, 2004, 40(17); 1079
- [28] Li C B, Mao R W, Zuo Y H, et al. 1.55 μm Ge islands resonant-cavity-enhanced detector with high-reflectivity bottom mirror. *Appl Phys Lett*, 2004, 85(14); 2697

硅基光子材料和器件的进展*

余金中[†] 王启明

(中国科学院半导体研究所, 北京 100083)

摘要: 评述硅基光子材料和器件的进展,包括硅二极管的受激发射、具有量子结构的 RCE(谐振腔增进型)光电二极管、MOS 高频光调制器、SOI 光开关阵列和可调谐波长滤波器,重点介绍低插入损耗、快响应的 SOI 基热光波导开关阵列的最新结果.以 SOI 为基片,成功地研制出带有全内反射(TIR)镜的重排无阻塞型光开关阵列,并首次研制出 16×16 阻塞型光开关阵列.在 $1.55 \mu\text{m}$ 波段,插入损耗和偏振相关性随着器件长度的增加而略微增大.如果器件的末端镀上抗反射膜,插入损耗会降低 $2 \sim 3 \text{dB}$,这些器件的上升和下降时间分别为 2.1 和 $2.3 \mu\text{s}$.

关键词: SOI; 光开关阵列; 光电二极管; 光互连

EEACC: 2500

中图分类号: TN25

文献标识码: A

文章编号: 0253-4177(2007)S0-0001-11

* 国家自然科学基金(批准号: 60336010), 国家重点基础研究发展规划(批准号: G2000-03-66)及国家高技术研究发展计划(批准号: 2002AA312060)资助项目

[†] 通信作者. Email: jzyu@red.semi.ac.cn

2006-12-20 收到, 2007-01-05 定稿